JACS
JOURNAL OF THE AMERICAN CHEMICAL SOCIETY
Communication
pubs.acs.org/JACS

Highly Electroconductive Mesoporous Graphene Nanofibers and Their Capacitance Performance at 4 V

Chaojie Cui, Weizhong Qian,* Yuntao Yu, Chuiyan Kong, Bo Yu, Lan Xiang, and Fei Wei*

Beijing Key Laboratory of Green Chemical Reaction Engineering and Technology, Department of Chemical Engineering, Tsinghua University, Beijing 100084, P. R. China

Supporting Information

ABSTRACT: We report the fabrication of one-dimensional highly electroconductive mesoporous graphene nanofibers (GNFs) by a chemical vapor deposition method using $MgCO_3{\cdot}3H_2O$ fibers as the template. The growth of such a unique structure underwent the first *in situ* decomposition of $MgCO_3{\cdot}3H_2O$ fibers to porous MgO fibers, followed by the deposition of carbon on the MgO surface, the removal of MgO by acidic washing, and the final self-assembly of wet graphene from single to double layer in drying process. GNFs exhibited good structural stability, high surface area, mesopores in large amount, and electrical conductivity 3 times that of carbon nanotube aggregates. It, used as an electrode in a 4 V supercapacitor, exhibited high energy density in a wide range of high power density and excellent cycling stability. The short diffusion distance for ions of ionic liquids electrolyte to the surface of GNFs yielded high surface utilization efficiency and a capacitance up to 15 $\mu F/cm^2$, higher than single-walled carbon nanotubes.

As one of important carbon nanomaterials, graphene has huge specific surface area (SSA), exohedral surface accessible to ions of electrolyte, excellent chemical stability, and potential application in clean electrochemical storage systems such as supercapacitor (SC).[1] To date, graphene was always large in size,[1,2] suffering from restacking between neighboring layers, due to the van der Waals force attraction. Consequently, it decreased the accessible surface area to ions of electrolytes, increased the diffusion resistance of ions, and degraded the performance of SCs significantly.[1b,3] These disadvantages became more significant when using ionic liquids (ILs) with larger ion size, compared to aqueous or organic electrolyte, as an electrolyte of SCs operated at 4 V to achieve a high energy density.[4] Creating an one-dimensional (1D) tubular or fiber structure of graphene would be effective to keep their dominant exohedral surface and to shorten the diffusion distance of ions of electrolyte in radial direction.[5] However, one should care to avoid the bundling of 1D materials with too small a diameter, i.e., like the graphene nanoribbons[6] or single-walled carbon nanotubes (SWCNTs),[7a,b] and to avoid the poor electrical conductivity of porous carbon materials, such as activated carbon (AC), carbide-derived carbons (CDC),[7c] or zeolite templated carbons (ZTC),[7d] both of which have remained great challenges for a long time.

We propose here, for the first time, the fabrication of highly electroconductive mesoporous graphene nanofibers (GNFs), 1D material on macroscopic scale, but 2D material composed of graphene with an average 2 layers on microscopic scale. The special structure was prepared by the decomposition of CH_4 over the template of $MgCO_3{\cdot}3H_2O$ fibers at 950 °C (Figure 1a). It

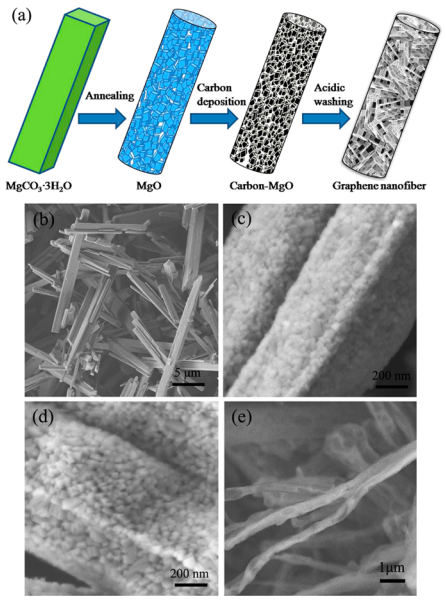

Figure 1. (a) Growth mode of GNFs. (b) SEM image of starting template of $MgCO_3{\cdot}3H_2O$ fibers. (c) Porous MgO fibers produced from the decomposition of $MgCO_3{\cdot}3H_2O$ fibers. (d) Carbon-MgO fibers produced from carbon deposition on MgO fibers. (e) SEM image of GNFs after removing MgO by acidic washing.

exhibited a SSA of 1280 m^2/g and mesopores in large amount. Its relatively large diameter of 100−500 nm allowed it to be free of bundling but offered the short diffusion distance for ions of electrolyte (1-ethyl-3-methylimidazolium tetrafluoroborate ($EMIBF_4$)). As a result, the capacitance value was 15 $\mu F/cm^2$ and 10.8 $\mu F/cm^2$ at current density of 0.5 and 10 A/g in a 4 V SC, respectively, higher than those of SWCNTs and graphene/SWCNT hybrid.[1,8] Energy density, based on GNF electrode, was 107 Wh/kg, higher than that of SWCNTs with SSA of 1100−2200 m^2/g.[8a,c] In addition, GNFs with high crystallinity exhibited

Received: December 8, 2013
Published: January 28, 2014

 © 2014 American Chemical Society dx.doi.org/10.1021/ja412219r | J. Am. Chem. Soc. 2014, 136, 2256−2259

excellent electrical conductivity (based on the powder), 3 times that of CNT powder, and very small resistance in SCs, which offered the excellent cycling stability of SCs. The special structure represented a new choice of electrode for next generation high voltage SCs.

Experimentally, the $MgCO_3{\cdot}3H_2O$ fibers with 200−1000 nm in diameter and SSA of 3.56 m^2/g (Figures 1b) were used as the starting template and annealed directly in the reactor (Figure S1). They were gradually decomposed with increasing temperature and were transformed into pure MgO fibers at 500 °C (Figures 1c and S2). During the process, the release of water at 164 °C and CO_2 at 438 °C resulted in the formation of many pores, which resulted in the SSA of MgO fibers increasing to 36 m^2/g. In the subsequent decomposition of CH_4 at 950 °C, the void of MgO network was deposited by carbon to form carbon-MgO fibers (Figures 1d and S3). The 1D macroscopic morphology of MgO fibers or carbon-MgO fibers was well kept in the processes above, which was crucial to prepare 1D GNFs (Figures 1e and 2) after the removal of MgO by acidic washing.

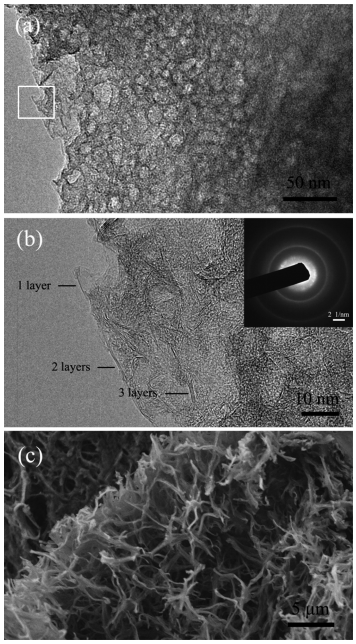

Figure 2. (a) TEM images of GNFs. (b) Enlarged magnification of white region in (a). Inset in (b) is the SAED. (c) SEM image of GNFs in large amounts.

TEM characterization (Figure 2a) indicated the high porosity of GNFs, which made GNFs nearly transparent under the electrical beam of TEM. These pores, left by removing MgO particles, had uniform diameter (10−20 nm) and uniform density (20−23 pores in the radial direction) along the axial direction of GNFs (Figures 2a,b and S3 and S5). Most of graphene were curved and followed the shape of original MgO crystals (Figure 2b). Compared to the wrinkled graphene with disordered pore, GNFs had relatively ordered pore structure, which was desirable as an electrode of SCs discussed below. The GNF was composed of 1−2 graphene layers dominantly (Figure 2b). Selected area electron diffraction (SAED) indicated its polycrystalline structure due to the small size and defective edge in large amounts (Figure 2b inset). The use of the template of $MgCO_3{\cdot}3H_2O$ fibers in large amounts was effective to produce GNFs in a large amount, of which the average length was ~10 μm and average diameter of 100−500 nm (Figure 2c). Since GNFs were prepared without the use of metal catalyst, its purity was close to 100% in TGA (Figure 3b) and 99.983% by ICP analysis

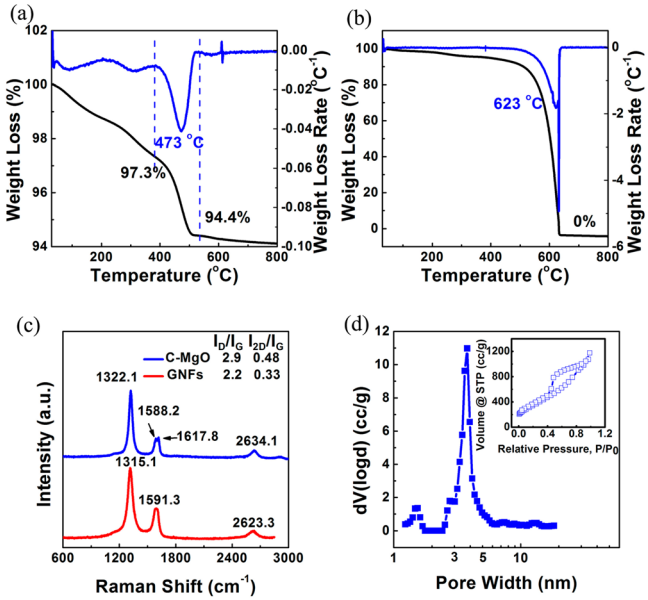

Figure 3. (a) TGA pattern of carbon-MgO fibers. (b) TGA pattern of GNFs. (c) Raman spectra of carbon-MgO fibers and GNFs. (d) Pore size distribution of GNFs and inset is isothermal curve in nitrogen adsorption.

(Table S1). XPS analysis suggested the oxygen content of GNFs was 0.68% (Figure S6), which was probably brought by the slight oxidation in acidic washing. However, the value was far lower than that (2−3%) of graphene from graphene oxide.[1] These results validated that the present method was effective to prepare GNFs with high purity.

In addition, the hole size (10−20 nm) of GNFs was smaller than the average size (100 nm) of MgO particles, and the average diameter (100−500 nm) of GNFs was smaller than that (200−1000 nm) of $MgCO_3{\cdot}3H_2O$ fibers. Apparently, wet GNFs underwent the volume shrinkage after drying. To study the structure evolution of GNFs, XRD, TGA, Raman, and nitrogen adsorption characterizations were made on carbon-MgO fibers and GNFs. XRD characterization suggested there was no peak response at 22−26° in both samples (Figure S4), indicating the carbon had a very thin layer. TGA analysis suggested that the burning temperature of carbon in carbon-MgO fibers was 473 °C (Figure 3a) but increased to 623 °C for GNFs (Figure 3b). We also validated that the burning temperature of multilayer graphene deposited on MgO surface was much higher (data not shown here). This suggested pristine carbon in carbon-MgO fibers was single layer graphene, which was overlapped to become 2 layer graphene in the drying process after removing MgO. Similarly, intensity ratio of 2D band (2621−2634 cm^{-1}) to G band (1588.4−1591.4 cm^{-1}) in Raman spectra (Figure 3c) decreased from 0.48 for carbon in carbon-MgO fibers to 0.33 for GNFs, also confirming the thickening of graphene layer. Intensity ratio of D band (1315−1323 cm^{-1}) to G band decreased from 2.9 for carbon in carbon-MgO fibers to 2.2 for GNFs, suggesting the amount of defective edge of graphene was decreased. The peak position of 2D band validated that it was a mixture of 1 and 2 layer graphene, since the peak position of most

dx.doi.org/10.1021/ja412219r | J. Am. Chem. Soc. 2014, 136, 2256−2259

2−4 layer graphene blue-shifted to 2650 cm^{-1} or much higher.[9] Moreover, nitrogen adsorption indicated that the carbon in carbon-MgO fibers had a surface area of 2411 m^2/g, a value very close to the theoretical one (2630 m^2/g) of single layer graphene (detailed calculation see SI-2). In sharp contrast, GNFs had a surface area of 1280 m^2/g, a value for typical 2 layer graphene. Characterization results of XRD, Raman, TGA, and nitrogen adsorption were all consistent and validated the self-assembly of graphene from 1 to 2 layers after drying. It was a first sample of 1D structure composed of 1−2 layer graphene prepared by hard template CVD method.

Although the drying of GNFs decreased their surface area, the interaction between curved graphene layers, whether in axial or radial direction, gave a robust structure, which was not destroyed after the long time ultrasonic treatment with the power of 3 kW. GNFs in large amounts were easily compressed (at 8 MPa) to give a packing density of 623 kg/m^3, larger than that (409 kg/m^3) of the powder of CNT with the diameter of 8−15 nm compressed at 10 MPa. It is possible to use GNFs to fabricate SCs with much higher volumetric energy density. GNFs exhibited higher electrical conductivity (compressed at 8 MPa) of 40 S/cm or 64 S* cm^2/g. The latter was about 3 times that of powder of CNTs above. Apparently, GNF was a bulk porous material with higher electroconductivity, compared to AC, CDC, and ZTC.

In addition, isothermal curve of nitrogen adsorption showed the trend of slow filling in adsorption in the entire pressure range and the rapid deadsorption in the middle pressure (Figure 3d inset), suggesting a typical ink-bottle-like pore structure.[1d,10] The pore size distribution of this product indicated it had the maximal peak at 3−5 nm, belonging to mesopores (Figure 3d). Pore volume of these mesopores was larger than that of 10−20 nm pores. In addition, the high purity of GNFs (Figure 3b, Table S1) suggested MgO could be easily solvable by acids, which implied that all carbon chambers in GNFs were fully accessible to ions. In addition, ions of electrolyte should diffuse along the channel (about micrometers long) between adjacent layers of large size graphene without holes.[1b] In comparison, GNFs with small diameter allowed the rapid diffusion of ions across their radial direction. These features were crucial to increase the performance of SCs as discussed below.

The material with huge SSA, large amount of mesopores, and high purity should be an ideal electrode for SCs at 4 V. Capacitance performances of GNF electrode in $EMIBF_4$ in a two-electrode cell were studied by scanning cyclical voltammograms (CV) at different scan rates (Figure 4a). They exhibited nearly the trapezoid-shaped CV curves below 200 mV/s, associated with the quantum capacitance of graphene flakes.[1g,11] Triangle zone in the right bottom was very small, indicating the insignificant redox reaction caused by impurities (oxygen, water, or metal). Specific capacitance was 193 F/g at 0.5 A/g (Figure 4c, Table S2). Although the value decreased with the increase of the current density,[4a,5b,8a] it was still higher than 140 F/g at 10A/g. The decreasing trend was not significant compared to a SWCNT sample with SSA of 1355 m^2/g and purity of 99.018% (Table S1), where capacitance was 125 F/g at 10A/g. Note here that the strong interaction of SWCNTs with ILs allowed the nearly monodispersion of SWCNTs in ILs,[12] and consequently, the outer surface of SWCNTs was nearly all accessible to ions of ILs electrolyte.[5a] GNFs had far larger volume and smaller SSA but exhibited the higher capacitance compared to SWCNTs above, which validated that most surface of GNFs was accessible to ions of ILs easily. Quantitatively, the capacitance based on SSA value

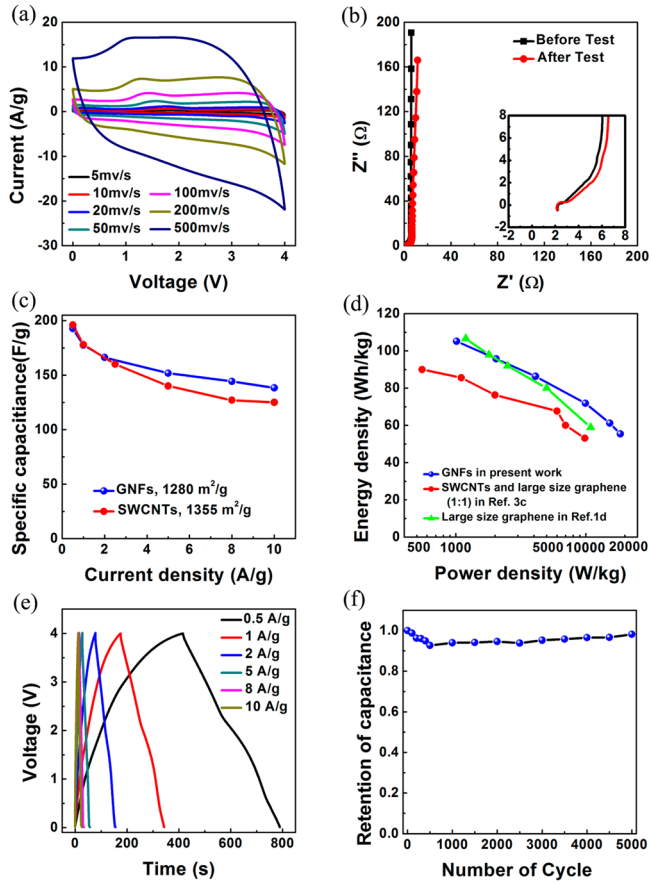

Figure 4. (a) CV curves of GNFs as electrode in 4 V SCs (two-electrode coin cell) using $EMIBF_4$ as electrolyte. (b) Nyquist plot for GNF electrode. (c) Comparison of specific capacitance of GNFs and SWCNTs (SI-3), obtained from the Galvanostatic charge−discharge curve, at different current densities. (d) Energy density at different power density. (e) Galvanostatic charge−discharge curve. (f) Retention of the relative capacitance of GNFs based SCs for 5000 cycle tests.

was 15 $\mu F/cm^2$ at 0.5 A/g for GNFs, higher than those (12−14 $\mu F/cm^2$) of SWCNTs (Figure 4c) and in ref 8a and much approaching the theoretical value (21 $\mu F/cm^2$) for graphene.[1g] Energy densities of GNFs were 103.5 and 70 Wh/kg at 1 and 10 kW/kg, respectively (Figure 4d). These values were apparently higher than those of large size graphene[1d] and composite of SWCNTs with large size graphene.[3c] In comparison, GNFs exhibited higher energy density in higher power density range of 5−20 kW/kg (Figure 3d, SI-4), further confirming the effect of short diffusion distance of ions across their radial direction on the rate performance of GNF electrode.

Galvanostatic charge−discharge test showed that charge and discharge times were 790, 344, 155, 57.4, 34.2, 27.4 s for the associated energy density of 105, 95.6, 86.3, 71.8, 61.2, and 55.4 Wh/kg, respectively (Figure 4e,d). That meant that the GNFs were capable of storing 71.8 Wh/kg energy and could be completely recharged in <1 min, shorter than the recharge time (2 min) to the same energy density for large size graphene.[1d] Equivalent series resistance before test and after test (Figure 4b) was similar and smaller than 2.2 Ω, far smaller than that (3.31 Ω) using large size graphene.[1d] The straight line in the low-frequency region in Nyquist plot (Figure 4b) suggested that process inside electrode was not ion diffusion limited and the SC behaved more like an ideal capacitor.[1d] Note that there was nearly no semi circle in the high-frequency region, indicating its

dx.doi.org/10.1021/ja412219r | J. Am. Chem. Soc. 2014, 136, 2256−2259

ultrasmall transfer resistance. The electrical resistance nearly did not change after CV scanning. This explained well the excellent charge and recharge ability of this SC and suggested the increased ion diffusion barrier under high current density was not due to the pore structure of electrode but to the intrinsic poor conductivity and the high viscosity of IL electrolyte.[4b]

Cycling stability of GNF-based SCs was tested at current density of 5 A/g for 5000 cycles (Figure 4f). The relative capacitance, based on the initial capacitance value, decreased to some degree in the first 500 cycles, probably due to the filling and wetting the ink-bottle pores to achieve a stable charge−discharge state. After that, the value recovered gradually, and the drop was only 1.81% after 5000 times tested. The cycling stability was better than that of a double-walled CNT (DWCNT) electrode as using the same separator with the same thickness[13] and was attributed to the efficient ion and electron diffusion channel of GNFs. The test of high temperature duration for GNF-based SCs was underway for evaluating their potential practical applications. From an engineering perspective, GNF has advantages over SWCNTs, DWCNTs, and large size graphene prepared from graphene oxide in free of bundling or restacking and in removing impurities (metal or oxygen) easily.[1,2b,c,8] In addition, the starting template was prepared by a very simple coprecipitation method in short time, and no complex hydrothermal step was needed. This allowed the scale-up synthesis of GNFs to be very easy and at low cost. In addition, the present method may be developed as a general way to use other nanosized 1D templates to prepare 1D GNFs with high porosity, excellent electrical conductivity, and short diffusion distance for ions for SCs operated at high voltage.

In summary, we successfully synthesized highly electroconductive mesoporous GNFs using 1D metal oxide fibers as the template in a CVD process. The preparation process of such a unique structure underwent the decomposition of starting template to become porous MgO fibers, followed by the deposition of carbon on MgO surface and the removal of MgO by acidic washing. The obtained sample exhibited good structural stability, high surface area, large amount of mesopores and low content of oxygen, excellent electrical conductivity, and, consequently, excellent capacitance performance at 4 V. Energy density and the capacitance value based on the surface area ranked among the highest values reported ever. The highly electroconductive mesoporous GNFs with large SSA but free of bundling were suitable for the use as electrodes in next generation SC with high energy density.

■ ASSOCIATED CONTENT

Supporting Information

Synthesis and characterization details. This material is available free of charge via the Internet at http://pubs.acs.org.

■ AUTHOR INFORMATION

Corresponding Authors

qianwz@tsinghua.edu.cn
wf-dce@tsinghua.edu.cn

Notes

The authors declare no competing financial interest.

■ ACKNOWLEDGMENTS

The authors thank the support of National 973 program (2011CB932602), NSFC program (21376135, 51236004).

■ REFERENCES

(1) (a) Zhu, Y. W.; Murali, S.; Stoller, M. D.; Ganesh, K. J.; Cai, W. W.; Ferreira, P. J.; Pirkle, A.; Wallace, R. M.; Cychosz, K. A.; Thommes, M.; Su, D.; Stach, E. A.; Ruoff, R. S. *Science* **2011**, *332*, 1537. (b) Yoo, J. J.; Balakrishnan, K.; Huang, J. S.; Meunier, V.; Sumpter, B. G.; Srivastava, A.; Conway, M.; Reddy, A. L. M.; Yu, J.; Vajtai, R.; Ajayan, P. M. *Nano Lett.* **2011**, *11*, 1423. (c) Choi, B. G.; Yang, M. H.; Hong, W. H.; Choi, J. W.; Huh, Y. S. *ACS Nano* **2012**, *6*, 4020. (d) Liu, C. G.; Yu, Z. N.; Neff, D.; Zhamu, A.; Jang, B. Z. *Nano Lett.* **2010**, *10*, 4863. (e) Yang, X. W.; Cheng, C.; Wang, Y. F.; Qiu, L.; Li, D. *Science* **2013**, *341*, 534. (f) Wang, H. L.; Liang, Y. Y.; Gong, M.; Li, Y. G.; Chang, W.; Mefford, T.; Zhou, J. G.; Wang, J.; Regier, T.; Wei, F.; Dai, H. J. *Nat. Commun.* **2012**, *3*, 917. (g) Xia, J. L.; Chen, F.; Li, J. H.; Tao, N. J. *Nat. Nanotechnol.* **2009**, *4*, 505.

(2) (a) Xu, Z.; Gao, C. *Nat. Commun.* **2011**, *2*, 571. (b) Ning, G. Q.; Fan, Z. J.; Wang, G.; Gao, J. S.; Qian, W. Z.; Wei, F. *Chem. Commun.* **2011**, *47*, 5976. (c) Chen, Z. P.; Ren, W. C.; Gao, L. B.; Liu, B. L.; Pei, S. F.; Cheng, H. M. *Nat. Mater.* **2011**, *10*, 424.

(3) (a) Wang, Y.; Wu, Y. P.; Huang, Y.; Zhang, F.; Yang, X.; Ma, Y. F.; Chen, Y. S. *J. Phys. Chem. C* **2011**, *115*, 23192. (b) Lee, J. H.; Park, N.; Kim, B. G.; Jung, D. S.; Im, K.; Hur, J.; Choi, J. W. *ACS Nano* **2013**, *7*, 9366. (c) Jha, N.; Ramesh, P.; Bekyarova, E.; Itkis, M. E.; Haddon, R. C. *Adv. Energy Mater* **2012**, *2*, 438.

(4) (a) Inagaki, M.; Konno, H.; Tanaike, O. *J. Power Sources* **2010**, *195*, 7880. (b) Hapiot, P.; Lagrost, C. *Chem. Rev.* **2008**, *108*, 2238. (c) Yang, L.; Fishbine, B. H.; Migliori, A.; Pratt, L. R. *J. Am. Chem. Soc.* **2009**, *131*, 12373. (d) Lazzari, M.; Mastragostino, M.; Pandolfo, A. G.; Ruiz, V.; Soavi, F. *J. Electrochem. Soc.* **2011**, *158*, A22. (e) Sillars, F. B.; Fletcher, S. I.; Mirzaeian, M.; Hall, P. J. *Energy Environ. Sci.* **2011**, *4*, 695.

(5) (a) Huang, J. S.; Sumpter, B. G.; Meunier, V.; Yushin, G.; Portet, C.; Gogotsi, Y. *J. Mater. Res.* **2010**, *25*, 1525. (b) Izadi-Najafabadi, A.; Futaba, D. N.; Iijima, S.; Hata, K. *J. Am. Chem. Soc.* **2010**, *132*, 18017.

(6) Li, X. L.; Wang, X. R.; Zhang, L.; Lee, S.; Dai, H. J. *Science* **2008**, *319*, 1229.

(7) (a) Khan, I. A.; Afrooz, A. R. M. N.; Flora, J. R. V.; Schierz, P. A.; Ferguson, P. L.; Sabo-Attwood, T.; Saleh, N. B. *Environ. Sci. Technol.* **2013**, *47*, 1844. (b) Zheng, C.; Qian, W. Z.; Yu, Y. T.; Wei, F. *Particuology* **2013**, *11*, 409. (c) Chmiola, J.; Largeot, C.; Taberna, P. L.; Simon, P.; Gogotsi, Y. *Science* **2010**, *328*, 480. (d) Kyotani, T.; Nagai, T.; Inoue, S.; Tomita, A. *Chem. Mater.* **1997**, *9*, 609.

(8) (a) Izadi-Najafabadi, A.; Yasuda, S.; Kobashi, K.; Yamada, T.; Futaba, D. N.; Hatori, H.; Yumura, M.; Iijima, S.; Hata, K. *Adv. Mater.* **2010**, *22*, E235. (b) Niu, Z. Q.; Zhou, W. Y.; Chen, J.; Feng, G. X.; Li, H.; Ma, W. J.; Li, J. Z.; Dong, H. B.; Ren, Y.; Zhao, D.; Xie, S. S. *Energy Environ. Sci.* **2011**, *4*, 1440. (c) Hiraoka, T.; Izadi-Najafabadi, A.; Yamada, T.; Futaba, D. N.; Yasuda, S.; Tanaike, O.; Hatori, H.; Yumura, M.; Iijima, S.; Hata, K. *Adv. Funct. Mater.* **2010**, *20*, 422. (d) Iwasaki, T.; Maki, T.; Yokoyama, D.; Kumagai, H.; Hashimoto, Y.; Asari, T.; Kawarada, H. *Phys. Status Solidi* **2008**, *2*, 53.

(9) (a) Hao, Y. F.; Wang, Y. Y.; Wang, L.; Ni, Z. H.; Wang, Z. Q.; Wang, R.; Koo, C. K.; Shen, Z. X.; Thong, J. T. L. *Small* **2010**, *6*, 195. (b) Rao, R.; Podila, R.; Tsuchikawa, R.; Katoch, J.; Tishler, D.; M. Rao, A.m.; Ishigami, M. *ACS Nano* **2011**, *5*, 1594. (c) Lui, C. H.; Li, Z. Q.; Chen, Z. Y.; Klimov, P. V.; Brus, L. E.; Heinz, T. F. *Nano Lett.* **2011**, *11*, 164. (d) Wu, Y. P.; Wang, B.; Ma, Y. F.; Huang, Y.; Li, N.; Zhang, F.; Chen, Y. S. *Nano Res.* **2010**, *3*, 661. (e) Ferrari, A. C.; Meyer, J. C.; Scardaci, V.; Casiraghi, C.; Lazzeri, M.; Mauri, F.; Piscanec, S.; Jiang, D.; Novoselov, K. S.; Roth, S.; Geim, A. K. *Phys. Rev. Lett.* **2006**, *97*, 187401.

(10) Ravikovitch, P. I.; Neimark, A. V. *Langmuir* **2002**, *18*, 9830.

(11) (a) Hahn, M.; Baertschi, M.; Barbieri, O.; Sauter, J.-C.; Kötz, R.; Gallay, R. *Electrochem. Solid-State Lett.* **2004**, *7*, A33. (b) Huang, J. S.; Qiao, R.; Feng, G.; Sumpter, B. G.; Meunier, V. In *Supercapacitors: Materials, Systems, and Applications*; Béguin, F.; Frackowiak, E., Eds.; Wiley-VCH: Weinheim, Germany, 2013; pp 191.

(12) Fukushima, T.; Kosaka, A.; Ishimura, Y.; Yamamoto, T.; Takigawa, T.; Ishii, N.; Ada, T. *Science* **2003**, *300*, 2072.

(13) Kong, C. Y.; Qian, W. Z.; Zheng, C.; Yu, Y. T.; Cui, C. J.; Wei, F. *Chem. Commun.* **2013**, *49*, 10727.